Determination of Refractive Index and Confinement Losses in Photonic Crystal Fibers Using FDFD Method: A Comparative Analysis

Faramarz E. Seraji[a] and F. Asghari[b]

[a]Optical Communication Group, Iran Telecom Research Center, Tehran, Iran
[b]Physics Group, Payam Noor University, Shahr Rey, Iran

Abstract— In this paper, we present a comparative numerical analysis to determine the refractive index of photonic crystal fibers (PCFs) by using FDFD method and used the results to evaluate the confinement losses of PCFs by considering the effects of air-hole rings in the cladding.

It is shown that by increasing the wavelength, the imaginary part of refraction index rises, resulting in increase of confinement losses nearly by order of 10. In lower wavelengths over the range of 0.2 to 1 μm, these losses were shown to be negligible. The obtained results show that as the number of air-hole ring in the cladding increases, the confinement losses over wavelengths would reduce. To show the effect of air-hole rings on confinement losses in PCFs, the FDFD method yielded accurate results that agree well with results of FEM method and source–model technique reported by others.

KEYWORDS: air-hole rings, confinement loss, finite difference frequency domain, refraction index, photonic crystal fibers

I. INTRODUCTION

Photonic crystal fibers (PCFs) are all-silica fibers that guide light by means of air-holes placed in the entire fiber length in the cladding [1]. The propagating modes of such fibers are leaky because the core refractive index is the same as the index beyond the finite cladding region. In addition to usual loss mechanisms as that of conventional fibers, there is loss mechanism peculiar to PCFs, known as confinement loss, which is due to presence of air-holes in their cladding [2-7]. The cladding of a PCF is usually comprised of hexagonally-packed rings of holes, and when the air-hole spacing Λ becomes comparable to the wavelength, several rings of holes are required to reduce the confinement loss to a practical value [8-9]. The presence of air-holes in the cladding causes the average refractive index in this region to reduce. Therefore, in order to optimize the design of PCFs for a minimum confinement loss, it is necessary to study the loss characteristics for an optimum PCF structure [10, 11].

Generally, for analysis of PCFs, due to their complex structures, numerical methods are used [11, 12]. To study the influence of number of air-hole rings on confinement loss of PCFs, we utilized fully vectorial finite-difference frequency domain (FDFD) method. In this method PCFs are considered with a finite cladding region of circular holes and full-vector modal calculations are performed. This method gives the complex propagation constant from which imaginary part is used for calculation of the confinement losses.

II. THE ANALYSIS

Various methods are utilized for analysis of photonic crystal fibers (PCFs). In all the solving methods, the Maxwell's equations are solved and the electric (E) and magnetic (H) fields are resolved into longitudinal components in Cartesian coordinate as follows:

$$\xi(x,y,z,t) = \xi_t(x,y) + \xi_z(x,y)\exp[-j(\omega t - \beta z)] \quad (1)$$

where β indicates the propagation constant and ξ is either E or H field. By replacing (1) in

Maxwell's equations, we obtain Helmholtz vectorial equations as:

$$\begin{cases} \left(\nabla_t^2 + k_0^2 n^2 - \beta^2\right) E_t = -\nabla_t \left(E_t \cdot \nabla_t \ln n^2\right) \\ \left(\nabla_t^2 + k_0^2 n^2 - \beta^2\right) H_t = \left(\nabla_t \times \mathbf{H_t}\right) \nabla \times \nabla_t \ln n^2 \\ \left(\nabla_t^2 + k_0^2 n^2 - \beta^2\right) E_z = j\beta E_t . \nabla_t \ln n^2 \\ \left(\nabla_t^2 + k_0^2 n^2 - \beta^2\right) H_z = \left(\nabla_t H_z + j\beta H_t\right) \cdot \nabla_t \ln n^2 \end{cases} \quad (2)$$

The above equations convert into eigen value problems for transmitting components of E and H fields. When the relative refractive index difference between core and cladding is small, the right hand side of (2) is negligible and can be approximated to zero, which is scalar approximation. Therefore, all the equations in (2) convert into one equation for either E or H field [11].

One point to note is that if the relative refractive index between core and cladding of PCF is high, the scalar approximation can be used to predict the propagation characteristics. Thus, a fully vectorial method is required for the analysis of PCFs. In this category, plane wave method (PWM), localized function method (LFM), finite difference time domain (FDTD) method, finite difference frequency domain (FDFD) method, multipole method (MPM) are relatively accurate methods for the analysis of PCFs [11].

In PWM, the magnetic field is expanded into plane waves and the core of PCF is assumed a solid cylindrical structure surrounded by periodic air-holes placed infinitely in the cladding region. Since, practically, the numbers of air-holes in the cladding are limited; this method is not suitable for the analysis of PCF [12]. For solving waveguide problems, LFM is used numerically as well as vectorially. In this method, the orthogonal functions such as sinusoidal, Lagurre-Gaussian (for 1D waveguides), Hermite-Gaussian (for 2D waveguides), are utilized. By applying periodic air-holes condition, the unknown modes are approximated by localized modes and are resolved into plane wave components, resulting in eigen value equation [13].

The FEM method is a accurate tool for solving waveguides problems which is normally based on simple solution of Helmholtz equations in frequency domain by dividing air-holes into triple cells [11]. This method, in spite of being accurate, has a complex algorithm that is hard to solve. In FDM method, the Yee mesh is utilized for solving electromagnetic problems in either time domain (FDTD) or frequency domain (FDFD). In comparison with other methods, FDM is more accurate and simpler.

Another simple and less accurate method is effective index method (EIM) in which an averaged refractive index of cladding with periodic air-hole is considered and modeled as an equivalent conventional step index single-mode fiber. In this method, by assuming air-hole as a unit cell, the scalar wave equation is solved to obtain mode field [14].

In FDTD method, the eigen frequency is solved for the given propagation constant. By FDFD method, which is based on direct solution of either Maxwell's or Helmholtz's equations, the attenuation of PCF can be determined. This method does not require second differentiation and thus six field components can be determined separately.

A. *FDFD method*

To solve Maxwell's equations by FDFD method, we utilize Yee mesh, as shown in Fig. 1 [15]. Let the time dependence of the field be represented as $exp\left[i\left(\beta z - \omega t\right)\right]$. Dividing E by $z_0 = \sqrt{\mu_0/\varepsilon_0}$ in Maxwell's equations $\left(\nabla \times \mathbf{E} = -\partial \mathbf{B}/\partial t \text{ and } \nabla \times \mathbf{H} = \varepsilon\, \partial \mathbf{E}/\partial t\right)$, we obtain:

$$\begin{cases} -ik_0 \varepsilon E_x = \dfrac{\partial H_z}{\partial y} - i\beta H_y \\ -ik_0 \varepsilon_r E_y = i\beta H_x - \dfrac{\partial H_z}{\partial x} \\ -ik_0 \varepsilon_r E_z = \dfrac{\partial H_y}{\partial x} - \dfrac{\partial H_x}{\partial y} \end{cases} \quad (3)$$

$$\begin{cases} -ik_0\varepsilon E_x = \dfrac{\partial H_z}{\partial y} - i\beta H_y \\ -ik_0\varepsilon_r E_y = i\beta H_x - \dfrac{\partial H_z}{\partial x} \\ -ik_0\varepsilon_r E_z = \dfrac{\partial H_y}{\partial x} - \dfrac{\partial H_x}{\partial y} \end{cases} \quad (4)$$

$$\begin{cases} -ik_0\varepsilon E_x = \dfrac{\partial H_z}{\partial y} - i\beta H_y \\ -ik_0\varepsilon_r E_y = i\beta H_x - \dfrac{\partial H_z}{\partial x} \\ -ik_0\varepsilon_r E_z = \dfrac{\partial H_y}{\partial x} - \dfrac{\partial H_x}{\partial y} \end{cases} \quad (5)$$

$$\begin{cases} -ik_0\varepsilon_{rx}(j,l)E_x(j,l) = \dfrac{H_z(j,l)-H_z(j,l-1)}{\Delta y} \\ \qquad\qquad -i\beta H_y(j,l) \\ -ik_0\varepsilon_{rx}(j,l)E_x(j,l) = \dfrac{H_z(j,l)-H_z(j,l-1)}{\Delta y} \\ \qquad\qquad -i\beta H_y(j,l) \\ -ik_0\varepsilon_{rz}(j,l)E_z(j,l) = \dfrac{H_y(j,l)-H_y(j-1,l)}{\Delta x} \\ \qquad\qquad -\dfrac{H_x(j,l)-H_x(j,l-1)}{\Delta y} \end{cases} \quad (6)$$

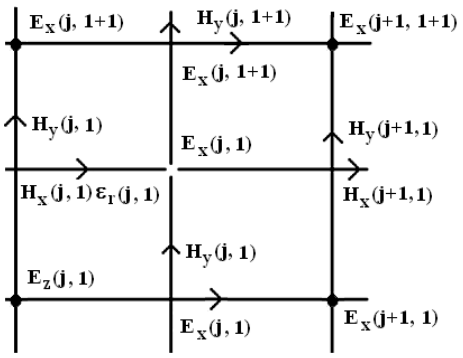

Fig. 1. Yee's mesh [15].

By using the following notations:

$$\begin{cases} \varepsilon_{rx}(j,l) = \left[\varepsilon_r(j,l) + \varepsilon_r(j,l-1)\right]/2 \\ \varepsilon_{ry}(j,l) = \left[\varepsilon_r(j,l) + \varepsilon_r(j,l) - \varepsilon_r(j-1,l)\right]/2 \\ \varepsilon_{rz}(j,l) = \left[\varepsilon_r(j,l) + \varepsilon_r(j-1,l-1) \right. \\ \qquad\qquad \left. + \varepsilon_r(j,l-1) + \varepsilon_r(j-1,l)\right]/4 \end{cases} \quad (7)$$

the expressions (3) to (6) can be simplified as:

$$ik_0\begin{bmatrix} H_x \\ H_y \\ H_z \end{bmatrix} = \begin{bmatrix} 0 & -i\beta I & U_y \\ i\beta I & 0 & -U_x \\ -U_y & U_x & 0 \end{bmatrix}\begin{bmatrix} E_x \\ E_y \\ E_z \end{bmatrix} \quad (8)$$

$$-ik_0\begin{bmatrix} \varepsilon_{rx} & 0 & 0 \\ 0 & \varepsilon_{ry} & 0 \\ 0 & 0 & \varepsilon_{rz} \end{bmatrix}\begin{bmatrix} E_x \\ E_y \\ E_z \end{bmatrix} = \begin{bmatrix} 0 & -i\beta I & V_y \\ i\beta I & 0 & -V_x \\ -V_y & V_x & 0 \end{bmatrix}\begin{bmatrix} H_x \\ H_y \\ H_z \end{bmatrix} \quad (9)$$

where I is a square unit matrix, and ε_{rx}, ε_{ry}, ε_{rz} are diagonal matrices determined by (7). The square matrices U_x, U_y, V_x, and V_y are evaluated under boundary condition. For example, if the values of window edge components in Yee's mesh tend to zero, the results are obtained as following matrices [15]:

$$U_x = \frac{1}{\Delta x}\begin{bmatrix} -1 & 1 & & & & \\ & -1 & 1 & & & \\ & & \ddots & \ddots & & \\ & & & \ddots & \ddots & \\ & & & & -1 & 1 \\ & & & & & -1 \end{bmatrix}$$

$$U_y = \frac{1}{\Delta y}\begin{bmatrix} -1 & & & 1 & & \\ & -1 & & & \ddots & \\ & & \ddots & & & \ddots \\ & & & \ddots & & 1 \\ & & & & \ddots & \\ & & & & -1 & \\ & & & & & 1 \end{bmatrix} \quad (10)$$

$$V_x = \frac{1}{\Delta x}\begin{bmatrix} 1 & & & & & \\ -1 & 1 & & & & \\ & -1 & \ddots & & & \\ & & \ddots & \ddots & & \\ & & & \ddots & \ddots & \\ & & & & -1 & 1 \\ & & & & & -1 \end{bmatrix}$$

$$V_y = \frac{1}{\Delta y}\begin{bmatrix} 1 & & & & & & \\ & 1 & & & & & \\ & & \ddots & & & & \\ & & & \ddots & & & \\ -1 & & & & \ddots & & \\ & & & & & 1 & \\ & & & & -1 & & 1 \end{bmatrix} \quad (11)$$

By some algebraic operations on (10) and (11), the eigenvalue equation for transverse electric field components will result as:

$$P\begin{bmatrix} E_x \\ E_y \end{bmatrix} = \begin{bmatrix} P_{xx} & P_{xy} \\ P_{yx} & P_{yy} \end{bmatrix}\begin{bmatrix} E_x \\ E_y \end{bmatrix} = \beta^2 \begin{bmatrix} E_x \\ E_y \end{bmatrix} \quad (12)$$

where the following notations are used:

$$\begin{aligned} P_{xx} &= -k_0^{-2}U_x\varepsilon_{rz}^{-1}V_yV_xU_y + \left(k_0^2 I + U_x\varepsilon_{rz}^{-1}V_x\right)\times \\ &\qquad \left(\varepsilon_{rx} + k_0^{-2}V_yU_y\right) \\ P_{yy} &= -k_0^2U_y\varepsilon_{rz}^{-1}V_xV_yU_x + \left(k_0^2 I + U_y\varepsilon_{rz}^{-1}V_y\right)\times \\ &\qquad \left(\varepsilon_{ry} + k_0^{-2}U_xV_x\right) \\ P_{xy} &= U_x\varepsilon_{rz}^{-1}V_y\left(\varepsilon_{ry} + k_0^{-2}V_xU_x\right) - k_0^{-2}\times \\ &\qquad \left(k_0^2 I + U_x\varepsilon_{rz}^{-1}V_x\right)V_yU_x \\ P_{yx} &= U_y\varepsilon_{rz}^{-1}V_x\left(\varepsilon_{rx} + k_0^{-2}V_yU_y\right) - k_0^{-2}\times \\ &\qquad \left(k_0^2 I + U_y\varepsilon_{rz}^{-1}V_y\right)V_xU_y \end{aligned} \quad (13)$$

where $E_{x,y}$ and $H_{x,y}$ are the x and y components of electric and magnetic fields, respectively [16]. In a similar procedure, the corresponding magnetic field equations can be derived as:

$$Q\begin{bmatrix} H_x \\ H_y \end{bmatrix} = \begin{bmatrix} Q_{xx} & Q_{yx} \\ Q_{yx} & Q_{yy} \end{bmatrix}\begin{bmatrix} H_x \\ H_y \end{bmatrix} = \beta^2 \begin{bmatrix} H_x \\ H_y \end{bmatrix} \quad (14)$$

The advantage of this approximation is that the H_t and E_t components can be determined separately and other E and H field components are obtained by (8) and (9). If material is neglected, the value of ε_r will be real and the matrix P converts into a real sparse matrix [15]. By applying boundary condition and solving (10), we calculate the propagation constant β. By using the relations $n_{eff}=\beta/k_0$ and $k_0=2\pi/\lambda_0$, where λ_0 is the free space wavelength, the effective refractive index is determined. In our analysis we used a PCF with a hexagonally-packed rings of holes as shown in Fig. 2, where Λ is the air-hole spacing and *d* is the air-hole diameter.

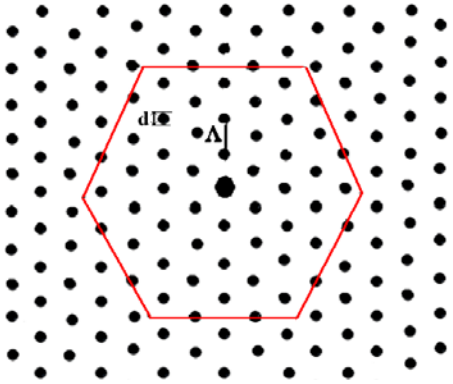

Fig. 2. PCF with a hexagonally-packed rings of holes.

The confinement loss of PCF can directly be evaluated by imaginary part of the effective refractive index obtained in FDFD method, i.e., in terms of dB/m is defined as [17]:

$$\alpha_L = \frac{20}{\ln(10)}\frac{2\pi}{\lambda}\mathrm{Im}\left(n_{\mathrm{eff}}\right)\cdot 10^9 \quad (15)$$

where the wavelength λ is in terms of nanometer.

III. Numerical Results

The effective refractive index for different PCF structures can be evaluated by FDFD method. In Fig. 3, we plotted the variations of effective refractive index as a function of number of grids selected in Yee's mesh at λ=1.55 μm for Λ=2.3 μm, *d*=2 μm, and n_{cl}=1.42. The calculating window in Yee's mesh was set to 8×8 μm.

For the given parameters values as above, we illustrated the effective index variation as a function of wavelength for number of grids of 40. We observe that as the wavelength increases, the effective index will lower down. In Fig. 4, with the same parameters values, the variation of effective refractive index is plotted with respect to wavelengths from 0.2

to 2 μm range. In Table 1, the values of effective refractive indices obtained by various methods are compared for Λ=2.3 μm at λ=1.55 μm. Among the results of compared methods, the results of MPM and FDFD methods almost tally with each other.

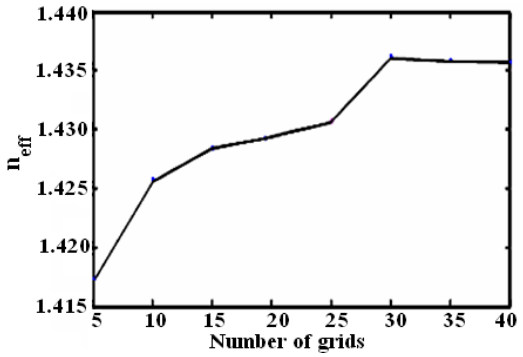

Fig. 3. Variation of effective refractive index vs. grid numbers.

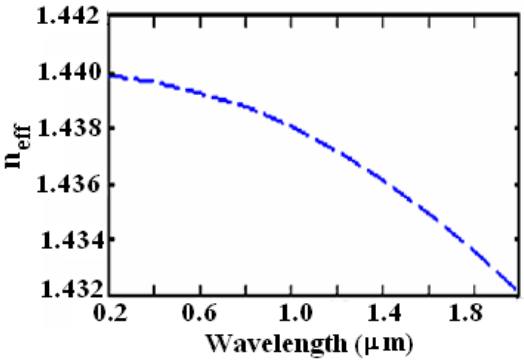

Fig. 4. Spectrum of the effective refractive index.

Table I. Comparison of effective indices obtained by different methods

Methods	FDFD	MPM [11]	PWM [12]	LFM [13]	EIM [14]
n_{eff}	1.4354	1.4353	1.4270	1.4230	1.4286

In Fig. 5, we have shown the real and imaginary parts of the refractive index versus wavelength. By increasing the wavelength, the imaginary part of refractive index rises while the real part lowers. In other word, when the wavelength increases, more fraction of light energy is confined in the cladding, thus resulting in more propagation loss, which is termed as confinement losses.

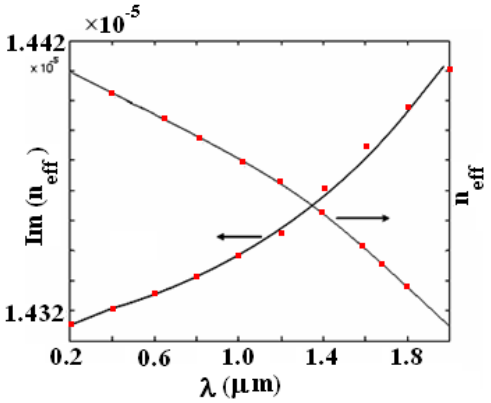

Fig. 5. Real and imaginary parts of the effective refractive indices.

In Fig. 6, the confinement losses for one ring of air-hole as a function of wavelength is depicted for d/Λ= 0.8. In shorter wavelengths over the range of 0.2 to 1 μm, this loss is negligible, but above this range, confinement losses increase rapidly, by order of 10. This result agrees well with that of [18] and [19], where FEM method was used. In [18], the confinement losses of a PCF with one air-hole ring in its cladding for Λ=2.3 μm at λ=1.55 μm, was of the order of 10^4 dB/m.

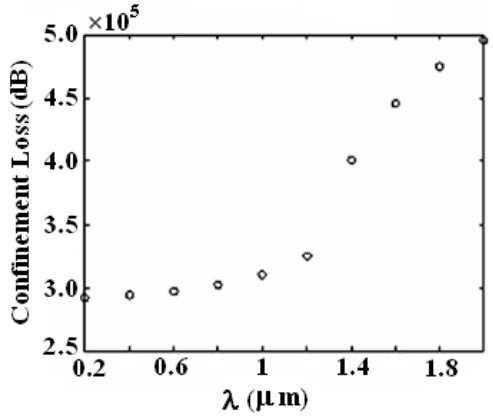

Fig. 6. Confinement losses spectrum for d/Λ=0.8.

By increasing the number of air-hole rings in the cladding of PCF, the confinement losses would decrease in such a way that it can be neglected in relative to other loss mechanisms in the PCF. In Fig. 7, we plotted the variations of confinement losses versus the ratio d/Λ for various number of air-holes in the cladding for Λ= 2.3 μm at 1.55 μm. We observe that confinement losses have decreasing nature with respect to the numbers air-hole rings. The

reason for reduction of confinement losses is that when the number of air-holes in the cladding of PCF increases, the effective refractive index of cladding will decrease, making the relative index difference between core and cladding to increase. As a result, more light energy will concentrate into core region, which in turn causes the confinement loss to decrease. Under this condition, mode guiding in PCF is carried out by total internal reflection rather than photonic band gap phenomenon.

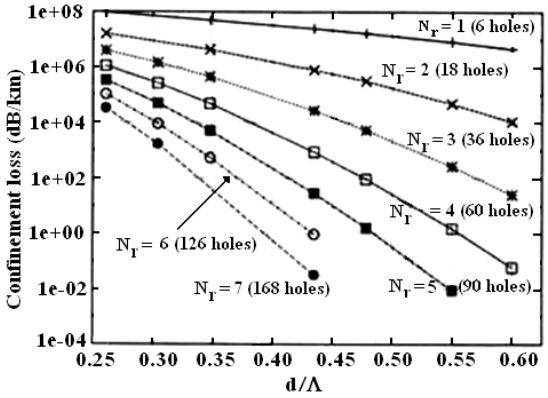

Fig. 7. Confinement loss versus d/Λ for different number of air-hole rings.

IV. CONCLUSION

A comparative numerical analysis, based on FDFD method, is presented to determine the refractive index of PCF and the obtained results are used to evaluate the confinement losses of PCFs by considering the effects of air-hole rings in the cladding.

Although in analytical effective index method sufficient design information can be obtained, the numerical methods are more accurate. The localized function method, which is based on direction solution of Maxwell's equations, the evaluation process leads to some complex integral equations. As well, the FEM method, in spite of being a accurate method, has the same problem complexity. The FDM method has the same accuracy as that of the FEM with a simpler mathematical operations. The frequency domain version of FDM, i.e., FDFD method has the advantage of direct solutions of Maxwell's or Helmholtz's equations to determine the losses in PCF. Moreover, in FDFD method performing second differentiations is not required and by using sparse technique the calculation time can be reduced.

On confinement losses analysis of PCFs. it is shown that by increasing the wavelength, the imaginary part of refraction index rises, resulting in increase of confinement losses nearly by order of 10. In lower wavelengths over the range of 0.2 to 1 μm, these losses were shown to be negligible, but above this range, confinement losses increases rapidly.

The variation of confinement losses over wavelengths for different number of air-hole rings have shown that as the number of air-holes rings increases, the confinement losses would reduce. In analyzing the effect of air-hole rings on confinement losses in PCFs, the FDFD method yielded accurate results that agree well with results of FEM method and source–model technique reported by others.

ACKNOWLEDGMENT

The authors acknowledge the Iran Telecommunication Research Center (ITRC) for financial support of this project.

REFERENCES

[1] T.A. Birks, J.C. Knight, and P. St. J. Russell, "Endlessly single-mode photonic crystal fiber," Opt. Lett., vol. 22, pp. 961-963, 1997.

[2] C. Martelli, J. Canning, B. Gibson, and S. Huntington, "Bend loss in structured optical fibers," Opt. Express, vol. 15, pp. 17639-17644, 2007.

[3] T. Sørensen, J. Broeng, A. Bjarklev, E. Knudsen, and S. E. B. Libori, "Macro-bending loss properties of photonic crystal fiber," Electron. Lett. vol. 37, pp. 287–289, 2001.

[4] J.C. Baggett, T.M. Monro, K. Furusawa, V. Finazzi, D.J. Richardson, "Understanding bending losses in holey optical fibers," Opt. Commun. vol. 227, pp. 317-335, 2003.

[5] N. Yi, A. Liang, X. Yuejian, Z. Lei, and P. Jiangde, "Confinement loss in solid-core

photonic bandgap fibers," Opt. Commun., vol. 235 pp. 305–310, 2004.

[6] M. Koshiba and K. Saitoh, "Simple evaluation of confinement losses in holey fibers," Opt. Commun., vol. 253, pp. 95–98, 2005.

[7] F.E. Seraji, M. Rashidi, and V. Khasheiel, "Parameter analysis of a photonic crystal fiber with raised-core index profile based on effective index method," Chin. Opt. Lett., vol. 4, pp. 442-445, 2006.

[8] L. Zhang, and C.X. Yang, "Photonic crystal fibers with squeezed hexagonal lattice," Opt. Express, vol. 12, pp. 2371-2376, 2004.

[9] A.B. Fedotov, S.O. Konorov, Y.N. Kondrat'ev, S.N. Bagayev, V.S. Shevandin, K.V. Dukel'skii, D.A. Sidorov-Biryukov, A.V. Khokhlov, V.B. Smirnov, and A.M. Zheltikov, "Measurement of optical losses for a family of microstructure fibers with a sequentially increasing number of hexagonal cycles of air holes," Laser Phys., vol. 13, pp. 856-860, 2003.

[10] M. Koshiba and K. Saitoh, "Structural dependence of effective area and mode field diameter for holey fibers," Opt. Express, vol. 11, pp. 1746-1756. 2003.

[11] S. Guo, F. Wu, S. Albin, H. Tai, and R.S.D. Rogowski, "Loss and dispersion analysis of microstructured fibers by finite-difference method," Opt. Express, vol. 12, pp. 3341-3351, 2004.

[12] E. Knudsen and A. Bjarklev, "Modeling photonic crystal fibers wih Hermit–Gaussian functions," Opt. Commu. Vol. 222, pp. 155–160, 2003.

[13] J. Arriaga, J.C. Knight, and P.St.J. Russell, "Modeling the propagation of light in photonic crystal fibers," Physica D, vol. 189, pp. 100-106, 2004.

[14] S.K. Varshney, M.P. Singh, and R.K. Sinha, "Propagation characteristics of photonic crystal fibers," Opt. Commun. vol. 24, pp. 192–198, 2003.

[15] Z. Zhu and T.G. Brown, "Full vectorial finite-difference analysis of microstructured optical fibers," Opt. Express, vol. 10, pp. 853-864, 2002.

[16] W. P. Huang and C. L. Xu, "Simulation of three-dimensional optical waveguides by a full-vector beam propagation method," IEEE J. Quant. Electron. Vol. 29, pp. 2639-2649, 1993.

[17] W.Y. Crutchfield., H. Cheng, and L. Greengard, "Sensitivity analysis of photonic crystal fiber," Opt. Express, vol. 12, pp.4220-4226, 2004.

[18] Y.C. Liu and Y. Lai "Optical birefringence and polarization dependent loss of square and rectangular," Opt. Express, vol. 3, pp.225-235, 2005.

[19] Hochman and Y. Leviatan, "Calculation of confinement losses in photonic crystal fibers by use of a source–model technique," J. Opt. Soc. Am. B, Vol. 22, pp. 474-480, 2005.

Faramarz E. Seraji was born in Ghaemshahr in green land of Mazadaran province, Iran. He graduated B.Sc Eng., M.Sc Eng. in communication engineering from Birla Institute of Technology (India), and PhD Eng. in optical fiber device and systems from Indian Institute of Technology (New Delhi, India), in 1983, 1985 and 1991, respectively. His major fields of interest are in optical fiber technology, photonic crystal fibers, fiber amplifiers, optical communications, next generation optical fibers, optical fibers devices and nanophotonics communications.

After graduation, he joined Optical Fiber Fabrication Co. in 1991 as a research scientist and in 1993 was appointed as Production Manager, with tenure of more than ten years. He was one among few other who started optical fiber fabrication in Iran. In his production-com-research activities managed a research work on "design and fabrication of dispersion-shifted fiber" which fetched his research group an innovation prize of tenth Kharazmi Festival. He supervised more than forty post graduate theses and published more than eighty journal and conference papers. In past years, he conducted a major project of Fabrication Photonic Crystal Fibers and involved in the project of Preform Fabrication

by VAD method at ITRC. He authored a book title as "Optical Communication: Fiber, Cable, and Device, (Chakameh Publication Co., Tehran, 2007); and translated two books titled as: Optical Fiber: Experiment and Measurement, (Imam Hossein Univ., 2005); Optical Fiber Communication (Baal Publication Co., Tehran, 2010).

Dr. Seraji has joined Iran Telecom Research Center (ITRC) in 2003 and currently is a faculty member of Optical Communication Group in Communication Technology Institute of ITRC. At present he is in charge of a project on "Design and Fabrication of Optical Filter Based on Photonic Crystal Fibers". Dr Seraji was Foundation Member Group of Optics and Photonics Society of Iran and recently has been appointed as Inspector of the Society for the second time.

Fatemeh Asghari was born in Arak, Central province, Iran. She graduated B.Sc and M.Sc. Physics from Arak University in 2001 and 2007, respectively. She has done her M.Sc. thesis in a joint project between ITRC and Physics Group of Arak University and worked on Characterization of Photonic Crystal Fibers. Her research fields of interest are photonic crystal fibers and optical fiber active and passive devices. At the present she is working on optical communication devices based on photonic crystal fibers. Miss Asghari is currently a faculty member of Payam Noor University, Shahr Rey, Iran.